Interacting electrons in a one-dimensional random array of scatterers – A Quantum Dynamics and Monte-Carlo study

V. Filinov[a,b], P. Thomas[b], I. Varga[b,c], T. Meier[b], M. Bonitz[d], V. Fortov[a], and S.W. Koch[b],
[a] *Institute for High Energy Density, Russian Academy of Sciences, Izhorskay 13/19, Moscow 127412, Russia*
[b] *Fachbereich Physik, Philipps-Universität Marburg, D-35032 Marburg, Germany*
[c] *Elméleti Fizika Tanszék, Budapesti Műszaki és Gazdaságtudományi Egyetem, H-1521 Budapest, Hungary*
[d] *Fachbereich Physik, Universität Rostock, Universitätsplatz 3, D-18051 Rostock, Germany*
(Dated: February 1, 2008)

The quantum dynamics of an ensemble of interacting electrons in an array of random scatterers is treated using a new numerical approach for the calculation of average values of quantum operators and time correlation functions in the Wigner representation. The Fourier transform of the product of matrix elements of the dynamic propagators obeys an integral Wigner-Liouville-type equation. Initial conditions for this equation are given by the Fourier transform of the Wiener path integral representation of the matrix elements of the propagators at the chosen initial times. This approach combines both molecular dynamics and Monte Carlo methods and computes numerical traces and spectra of the relevant dynamical quantities such as momentum-momentum correlation functions and spatial dispersions. Considering as an application a system with fixed scatterers, the results clearly demonstrate that the many-particle interaction between the electrons leads to an enhancement of the conductivity and spatial dispersion compared to the noninteracting case.

I. INTRODUCTION

Noninteracting electrons in an array of fixed random scatterers are known to experience Anderson localization at temperature $T = 0$ in one-dimensional systems. In two-dimensional systems single-parameter scaling theory predicts that all states are localized as well [1]. In three-dimensional arrays of random scatterers localization appears at the band extremities, while the center may consist of delocalized states, indicating a disorder driven metal-insulator transition in three dimensions only.

This picture has been challenged by recent experiments, which suggest a metal-insulator transition also in disordered two-dimensional electron systems [2]. A theoretical explanation [3] indicated that the Coulomb interaction between the electrons plays a central role in this effect. Moreover, the experimental study of persistent currents in mesoscopic metal rings [4] yields currents that are two orders of magnitude larger than predicted by theories based on noninteracting electrons [5]. These findings suggest that it is the many-particle interaction which leads to delocalization tendencies. To the best of our knowledge this has first been suggested by M. Pollak and coworkers [6, 7].

Evidence for this influence of the Coulomb interaction has been obtained by examining the problem of two interacting electrons in a one-dimensional disordered band [8]. It is, however, not clear whether this schematic model is able to yield answers for more realistic systems described by an ensemble of many electrons. Therefore, attempts have been made to calculate directly the conductivity of a disordered system of many electrons. Numerical results for the ensemble averaged logarithm of the conductance have been obtained for small systems by applying a Hartree-Fock based diagonalization scheme for electrons without [9, 10] and with spin [11]. An increase of the conductivity for certain regions in the disorder-interaction parameter space has been demonstrated in these publications.

The purpose of this paper is two-fold: i) We present our approach, which does not rely on small system sizes. This can be applied to a wide variety of different physical systems, such as plasmas, liquids, and solids. ii) As an illustration we study the problem described above. In particular, in this paper we investigate the influence of the many-particle interaction on electronic transport. We consider as a case study a one-dimensional disordered array of scatterers interacting repulsively with the electron system. Without electron-electron interaction such a system shows Anderson localization. It is the purpose of this application to study the effect of the long-range electron-electron Coulomb interaction on the mobility of the electrons.

Anderson localization at temperature $T = 0$ relies on quantum coherence of electron trajectories and results from interference. The key parameter in the physics of electron interference phenomena is the dephasing time of electrons. At finite temperatures the electron coherence is destroyed by both the electron-electron and the phonon-electron scattering [12, 13, 14, 15]. To study the influence of these effects on kinetic electron properties in a random environment

we have simulated the quantum dynamics in a one-dimensional canonical ensemble at finite temperature for both interacting and noninteracting electrons using a Quantum-Dynamics-Monte-Carlo scheme. The main quantities calculated in this paper are the temporal momentum-momentum correlation functions, their frequency-domain Fourier transforms and the time dependence of the spatial dispersions. We discovered that the results strongly depend on the electron-electron interaction, clearly demonstrating the delocalizing influence of the many-particle interaction even at finite temperatures.

Our approach also treats the positions of the scattering centers as dynamical variables. We are therefore in the position to generate various initial conditions, including the scenario of "electron bubbles" as an interesting side-result.

We start in Section II by presenting the Quantum-Dynamics-Monte-Carlo approach used in this work, which is based of the Wigner representation of quantum statistical mechanics. It treats both electrons and scatterers on an equal footing. Details of our model, relevant correlation functions and the system of reduced units are introduced in Section III. Numerical results for the momentum-momentum correlation function in the time and frequency domains and for the spatial dispersion are given in Section IV. Finally, Section V contains a discussion of our results.

II. WIGNER REPRESENTATION OF TIME CORRELATION FUNCTIONS

According to the Kubo formula the conductivity is the Fourier transform of the current–current correlation function. Generally, time correlation functions $C_{FA}(t) = \left\langle \hat{F}(0)\hat{A}(t) \right\rangle$ for a pair of dynamic variables $F(t) = \left\langle \hat{F}(t) \right\rangle$ and $A(t) = \left\langle \hat{A}(t) \right\rangle$ are among the most interesting quantities in the study of the dynamics of electrons in disordered systems of scatterers, such as transport coefficients, chemical reaction rates, equilibrium and transient spectroscopy, etc. Our starting point is the general operator expression for the canonical ensemble-averaged time correlation function [16]:

$$C_{FA}(t) = Z^{-1}\mathrm{Tr}\left\{ \hat{F}\, e^{i\hat{H}t_c^*/\hbar}\, \hat{A}\, e^{-i\hat{H}t_c/\hbar} \right\}, \tag{1}$$

where $\hat{H}$ is the Hamiltonian of the system expressed as a sum of the kinetic energy operator, $\hat{K}$, and the potential energy operator, $\hat{U}$. Time is taken to be a complex quantity, $t_c = t - i\hbar\beta/2$, where $\beta = 1/k_BT$ is the inverse temperature with k_B denoting the Boltzmann constant. The operators $\hat{F}$ and $\hat{A}$ are quantum operators of the dynamic quantities under consideration and $Z = \mathrm{Tr}\left\{ e^{-\beta\hat{H}} \right\}$ is the partition function.

The Wigner representation of the time correlation function in a υ–dimensional space can be written as:

$$C_{FA}(t) = (2\pi\hbar)^{-2\upsilon} \int\int d\mu_1 d\mu_2\, F(\mu_1)\, A(\mu_2)\, W(\mu_1;\mu_2;t;i\hbar\beta), \tag{2}$$

where we introduce the short-hand notation for the phase space point, $\mu_i = (p_i, q_i), (i = 1, 2)$, and p and q comprise the momenta and coordinates, respectively, of all particles in the system. In the definition (2), $W(\mu_1;\mu_2;t;i\hbar\beta)$ is the spectral density expressed as

$$\begin{aligned} W(\mu_1;\mu_2;t;i\hbar\beta) \;=\; & Z^{-1} \int\int d\xi_1 d\xi_2\, e^{i\frac{p_1\xi_1}{\hbar}} e^{i\frac{p_2\xi_2}{\hbar}} \times \\ & \times \left\langle q_1 + \frac{\xi_1}{2} \left| e^{i\hat{H}t_c^*/\hbar} \right| q_2 - \frac{\xi_2}{2} \right\rangle \left\langle q_2 + \frac{\xi_2}{2} \left| e^{-i\hat{H}t_c/\hbar} \right| q_1 - \frac{\xi_1}{2} \right\rangle, \end{aligned} \tag{3}$$

and $A(\mu)$ denotes Weyl's symbol [17] of the operator $\hat{A}$

$$A(\mu) = \int d\xi\, e^{-i\frac{p\xi}{\hbar}} \left\langle q - \frac{\xi}{2} \left| \hat{A} \right| q + \frac{\xi}{2} \right\rangle, \tag{4}$$

and similarly for the operator $\hat{F}$. Hence the problem of the numerical calculation of the canonically averaged time correlation function is reduced to the computation of the spectral density.

To obtain the integral equation for W let us introduce the a pair of dynamic p,q-trajectories $\{\bar{q}_\tau(\tau;p_1,q_1,t),\, \bar{p}_\tau(\tau;p_1,q_1,t)\}$ and $\{\tilde{q}_\tau(\tau;p_2,q_2,t),\, \tilde{p}_\tau(\tau;p_2,q_2,t)\}$ starting at $\tau = t$ from the initial condition $\{q_1, p_1\}$ and $\{q_2, p_2\}$ propagating in 'negative' and 'positive' time direction, respectively:

$$\begin{aligned} & \frac{d\bar{p}}{d\tau} = \frac{1}{2}F\left[\bar{q}_\tau(\tau)\right]; \qquad \frac{d\bar{q}}{d\tau} = \frac{\bar{p}_\tau(\tau)}{2m}, \\ \text{with} \qquad & \bar{p}_t(\tau = t;p_1,q_1,t) = p_1; \qquad \bar{q}_t(\tau = t;p_1,q_1,t) = q_1, \end{aligned} \tag{5}$$

and

$$\begin{array}{lll} & \frac{d\tilde{p}}{d\tau} = -\frac{1}{2}F\left[\tilde{q}_\tau(\tau)\right]\,; & \frac{d\tilde{q}}{d\tau} = -\frac{\tilde{p}_\tau(\tau)}{2m}, \\ \text{with} & \bar{p}_t(\tau = t; p_1, q_1, t) = p_1\,; & \tilde{q}_t(\tau = t; p_1, q_1, t) = q_1, \end{array} \tag{6}$$

$$\text{while} \quad \varpi(s,q) = \frac{4}{(2\pi\hbar)^\upsilon \hbar}\int dq'\,\tilde{U}(q-q')\sin\left(\frac{2sq'}{\hbar}\right) + F(q)\nabla\delta(s), \tag{7}$$

$\delta(s)$ is the Dirac delta function and $F\left(q\right) \equiv -\nabla\tilde{U}$ with $\tilde{U}$ being the total potential.

Then as has been proved in [18, 19] the W obeys the following integral equation:

$$\begin{aligned} W(\mu_1;\mu_2;t;i\hbar\beta) \;&=\; \bar{W}(\bar{p}_0,\bar{q}_0;\tilde{p}_0,\tilde{q}_0;i\hbar\beta) + \\ &+\; \frac{1}{2}\int_0^t d\tau \int ds\, W(\bar{p}_\tau - s, \bar{q}_\tau; \tilde{p}_\tau, \tilde{q}_\tau; \tau; i\hbar\beta)\,\varpi(s,\bar{q}_\tau) - \\ &-\; \frac{1}{2}\int_0^t d\tau \int ds\, W(\bar{p}_\tau, \bar{q}_\tau; \tilde{p}_\tau - s, \tilde{q}_\tau; \tau; i\hbar\beta)\,\varpi(s,\tilde{q}_\tau), \end{aligned} \tag{8}$$

where equation (8) has to be supplemented by an initial condition for the spectral density, $\bar{W}(\mu_1;\mu_2;i\hbar\beta) \equiv W(\mu_1;\mu_2;t=0;i\hbar\beta)$, which can be expressed in the form of a finite difference approximation of the path integral [18, 19, 20]:

$$\bar{W}\left(\mu_1;\mu_2;i\hbar\beta\right) \approx \int\int d\tilde{q}_1 \ldots d\tilde{q}_n \int\int dq'_1 \ldots dq'_n\, \Psi\left(\mu_1;\mu_2;\tilde{q}_1,\ldots,\tilde{q}_n;q'_1,\ldots,q'_n;i\hbar\beta\right), \tag{9}$$

$$\begin{aligned} &\text{with} \quad \Psi\left(\mu_1;\mu_2;\tilde{q}_1,...,\tilde{q}_n;q'_1,...,q'_n;i\hbar\beta\right) \equiv \\ &\frac{1}{Z}\left\langle q_1\left|e^{-\epsilon\hat{K}}\right|\tilde{q}_1\right\rangle e^{-\epsilon U(\tilde{q}_1)}\left\langle \tilde{q}_1\left|e^{-\epsilon\hat{K}}\right|\tilde{q}_2\right\rangle e^{-\epsilon U(\tilde{q}_2)}\;\ldots\; e^{-\epsilon U(\tilde{q}_n)}\left\langle \tilde{q}_n\left|e^{-\epsilon\hat{K}}\right|q_2\right\rangle \varphi\left(p_2;\tilde{q}_n,q'_1\right)\times \\ &\left\langle q_2\left|e^{-\epsilon\hat{K}}\right|q'_1\right\rangle e^{-\epsilon U(q'_1)}\left\langle q'_1\left|e^{-\epsilon\hat{K}}\right|q'_2\right\rangle e^{-\epsilon U(q'_2)}\ldots e^{-\epsilon U(q'_n)}\left\langle q'_n\left|e^{-\epsilon\hat{K}}\right|q_1\right\rangle \varphi\left(p_1;q'_n,\tilde{q}_1\right), \end{aligned} \tag{10}$$

$$\text{where} \quad \varphi\left(p;q',q''\right) \equiv \left(2\lambda^2\right)^{\upsilon/2}\exp\left[-\frac{1}{2\pi}\left\langle \frac{p\lambda}{\hbar} + i\pi\frac{q'-q''}{\lambda}\;\middle|\;\frac{p\lambda}{\hbar} + i\pi\frac{q'-q''}{\lambda}\right\rangle\right], \tag{11}$$

where $\langle x|y\rangle$ denotes the scalar product of two vectors $\vec{x}\cdot\vec{y}$. In this expression the original (unknown) density matrix of the correlated system $e^{-\beta(\hat{K}+\hat{U})}$ has been decomposed into $2n$ factors, each at a $2n$ times higher temperature, with the inverse $\epsilon = \beta/2n$ and the corresponding high temperature DeBroglie wave length squared $\lambda^2 \equiv 2\pi\hbar^2\epsilon/m$. This leads to a product of known high-temperature (weakly correlated) density matrices, however, at the price of $2n$ additional integrations over the intermediate coordinate vectors (over the "path"). This representation is exact in the limit $n\to\infty$, and for finite n an error of order $1/n$ occurs.

Expression (10) has to be generalized to properly account for spin effects. This gives rise to an additional spin part of the density matrix, whereas exchange effects can be accounted for by the antisymmetrization of only one off-diagonal matrix element in (10). As a result, in (10) one matrix element, for example $\left\langle q'_1\left|e^{-\epsilon\hat{K}}\right|q'_2\right\rangle$ has to be replaced by the antisymmetrized expression $\left\langle q'_1\left|e^{-\epsilon\hat{K}}\right|q'_2\right\rangle_A$ which can be written as the following sum of determinants involving the *single-particle* density matrix

$$\left\langle q'_1\left|e^{-\epsilon\hat{K}}\right|q'_2\right\rangle_A \equiv \sum_{s=0}^{N} C_N^s \det\left|\left\langle q'_{1,a}\left|e^{-\epsilon\hat{k}}\right|q'_{2,b}\right\rangle\right|_s = \sum_{s=0}^{N} C_N^s \det\left|e^{-\frac{\pi}{\lambda^2}\left|q'_{1,a}-q'_{2,b}\right|^2}\right|_s. \tag{12}$$

Here $C_N^s \equiv N!/s!(N-s)!$, and $|q'_{1,a} - q'_{2,b}|$ denotes the distance between the vertices q'_1 and q'_2 of particles a and b, respectively. As a result of the summation over spin variables and all possible exchange permutations, the determinant carries a subscript s denoting the number of electrons having the same spin projection. To improve the accuracy of the obtained expression, in the total potential U being the sum of all pair interactions U_{ab}, we will replace $U_{ab} \to U_{ab}^{\text{eff}}$ where U_{ab}^{eff} is the proper effective quantum pair potential, see below. For more details on the path integral concept,

we refer to Refs. [21, 22, 23, 24, 25], for recent applications of this approach to correlated Coulomb systems, cf. [26, 27, 28, 29].

Let us now come back to the integral equation (8). One readily checks that its solution can be represented symbolically by an iteration series of the form

$$\begin{aligned} W^t &= \bar{W}^t + K^t_\tau W^\tau \\ &= \bar{W}^t + K^t_{\tau_1}\bar{W}^{\tau_1} + K^t_{\tau_2}K^{\tau_2}_{\tau_1}\bar{W}^{\tau_1} + K^t_{\tau_3}K^{\tau_3}_{\tau_2}K^{\tau_2}_{\tau_1}\bar{W}^{\tau_1} + \ldots, \end{aligned} \tag{13}$$

where $\bar{W}^t$ and $\bar{W}^{\tau_1}$ are the initial quantum spectral densities evolving classically during time intervals $[0,t]$ and $[0,\tau_1]$, respectively, whereas $K^{\tau_{i+1}}_{\tau_i}$ are operators that govern the propagation from time τ_i to τ_{i+1}.

Since the time correlation functions (1) are linear functionals of the spectral density, for them the same series representation holds,

$$\begin{aligned} C_{FA}(t) = (2\pi\hbar)^{-2\upsilon}\int\int d\mu_1 d\mu_2\, \phi(\mu_1;\mu_2)\, W(\mu_1;\mu_2;t;i\hbar\beta) \equiv \big(\phi|W^t\big) = \\ \big(\phi|\bar{W}^t\big) + \big(\phi|K^t_{\tau_1}\bar{W}^{\tau_1}\big) + \big(\phi|K^t_{\tau_2}K^{\tau_2}_{\tau_1}\bar{W}^{\tau_1}\big) + \big(\phi|K^t_{\tau_3}K^{\tau_3}_{\tau_2}K^{\tau_2}_{\tau_1}\bar{W}^{\tau_1}\big) + \ldots \end{aligned} \tag{14}$$

where $\phi(\mu_1;\mu_2) \equiv F(\mu_1)A(\mu_2)$ and the parentheses $(\ldots|\ldots)$ denote integration over the phase spaces $\{\mu_1;\mu_2\}$ as indicated in the first line of the equation.

Note that the mean value $\bar{F}(t)$ of a quantum operator $\hat{F}$ can be represented in a form analogous to (14):

$$\bar{F}(t) = (2\pi\hbar)^{-2\upsilon}\int\int d\mu_1 d\mu_2\, \frac{F(\mu_1)+F(\mu_2)}{2}\, W(\mu_1;\mu_2;t;i\hbar\beta), \tag{15}$$

which allows us to increase the efficiency of the simulations. In the following Section we apply this scheme to a system of interacting electrons and random scatterers.

III. QUANTUM DYNAMICS

As an application, in this work we will consider a system composed of heavy particles (called scatterers) with mass m_s and negatively charged electrons with mass m_e. To avoid bound state effects due to attraction we consider in this case study only negatively charged scatterers, assuming a positve backgroud for charge neutrality. The influence of electron-scatterer attraction will be studied in a further publication.

The possibility to convert a series like (14) into a form convenient for probabilistic interpretation allows us to apply Monte Carlo methods to its evaluation. According to the general theory of the Monte Carlo methods for solving linear integral equations, e.g. [30], one can simultaneously calculate all terms of the iteration series (14). Using the basic ideas of [30] we have developed a Monte Carlo scheme, which provides domain sampling of the terms giving the main contribution to the series (14), cf. [18, 19]. This sampling also reduces the numerical expenses for calculating the integrals in each term. For simplicity, in this work, we take into account only the first term of iteration series (14), which is related to the propagation of the initial quantum distribution (11) according to the Hamiltonian equation of motion. This term, however, does not describe pure classical dynamics but accounts for quantum effects [31] and, in fact, contains arbitrarily high powers of Planck's constant. The remaing terms of the iteration series describe momentum jumps [18, 19, 32] which account for higher-order corrections to the classical dynamics of the quantum distribution (11) which are expected to be relevant in the limit of high density. A detailed investigation of the conditions for which the contribution of the next terms of the iteration series should be taken into account is presented in [32, 33].

The dynamical evolution of this system is studied along the trajectory pair in phase space, Eqs. (5) and (6), on time scales less than a maximum time t'. This time is chosen small enough such that the system of scatterers is practically stationary within the time interval $0 \le t < t'$. The initial states of the system evolution are proper equilibrium states and thus relate to physical times much larger than t'. So the initial micro states (particle configurations in phase space) can be randomly generated and an ensemble averaging should be performed with the canonical density operator of the electron-scatterer system, where the latter has been computed by the path integral Monte-Carlo method NEW [21] according to the probability distribution, which is proportional to $|\Psi|$ (10). So due to the time reversibility it is more convenient to start generation of the trajectories (Eqs. (5) and (6)) from time $\tau = 0$ starting from sampled by Monte Carlo method initial particle configurations (points t_j on Fig.1). The phase cofactor of the complex-valued function Ψ was taken into account by introducing the weight function [30, 34, 35] of the initial configurations for the subsequent dynamic evolution. In principle, the method is also applicable to liquids or plasmas by assigning smaller masses to the scatterers.

This approach allows us to generate, in a controlled way, various kinds of initial conditions of the many-body system, in particular (i) those which are characteristic of the fully interacting system [i.e.including scatterer-scatterer (s-s), electron-scatterer (e-s), and electron-electron (e-e)] and (ii) those which result if some aspects of these interactions are ignored. In all cases, the short-time dynamics can then be followed by including or excluding the (e-e)-interaction.

For the numerical calculations we introduce dimensionless units, using the maximum value of the time characteristic for the short-time dynamics, t' as the unit of the dynamic time t of the system. So the dimensionless time defined by $\theta = t/t'$ will always vary between 0 and 1. As a unit of length we take the reciprocal wavenumber k^{-1}, determined by the ratio $k^2 = 2m_eE_0/\hbar^2$. E.g., for one electron in an external potential field $\tilde{U} = V_0U(q)$ the operator exponent of the time evolution propagator $\exp(-i\hat{H}t/\hbar)$ can be rewritten in the form

$$\frac{\hat{H}t}{\hbar} = \left\{-\frac{\hbar^2}{2m_e}\Delta + V_0U(q)\right\}\frac{t}{\hbar} = \left\{-\frac{1}{2M}\Delta + \xi_0U(q)\right\}\theta \tag{16}$$

where Δ is the Laplace operator, V_0 is characteristic strength of the interaction potential, $M = \hbar/2E_0t'$, $\xi_0 = V_0/2E_0M = V_0t'/\hbar$.

The tensor of the electrical conductivity is given by:

$$\sigma_{\alpha\gamma}(\omega) = \int_0^\infty dt\, e^{i\omega t-\epsilon t}\int_0^\beta d\lambda\,\left\langle \hat{J}_\gamma\hat{J}_\alpha(t+i\hbar\lambda)\right\rangle \tag{17}$$

according to the quantum Kubo formula [16], where $\epsilon \to +0$. The current operator is

$$\hat{J}_\alpha = \sum_{i=1}^{N_e} e\dot{q}_i^\alpha(t) = \sum_{i=1}^{N_e}\frac{e}{m_e}p_i^\alpha, \tag{18}$$

with $\dot{q}^\alpha$ being the $\alpha-$component of the velocity operator of the electron. In the Wigner representation this tensor reads

$$\sigma_{\alpha\gamma}(\omega) = \int_0^\infty dt\, e^{i\omega t-\epsilon t}\int_0^\beta d\lambda\,\phi_{\alpha\gamma}(t,\lambda) \equiv \frac{k^2}{e^2}\frac{\tilde{\sigma}_{\alpha\gamma}(\omega)}{2E_0t'} \tag{19}$$

where

$$\phi_{\alpha\gamma}(t,\lambda) = \left\langle \hat{J}_\gamma\hat{J}_\alpha(t+i\hbar\lambda)\right\rangle = (2\pi\hbar)^{-2\nu}\int d\mu_1 d\mu_2\, J_\gamma(\mu_1)J_\alpha(\mu_2)W(\mu_1;\mu_2;t;i\hbar\beta;i\hbar\lambda), \tag{20}$$

and the spectral density $W(\mu_1;\mu_2;t;i\hbar\beta;i\hbar\lambda)$ is defined as in Eq. (3) by replacing t_c^* by $\tau_1 = t_1 + i\hbar\lambda$, and t_c by $\tau_2 = t_2 - i\hbar(\beta-\lambda)$. The dimensionless conductivity tensor is denoted by $\tilde{\sigma}_{\alpha\gamma}(\omega)$.

Our model of correlated electrons interacting with an array of random scatterers is described by the following Hamiltonian,

$$\begin{aligned}
\hat{H} &= \hat{H}_e + \hat{H}_{es} + \hat{H}_{ss} = (\hat{K}_e + \tilde{U}_{ee}) + \tilde{U}_{es} + (\hat{K}_s + \tilde{U}_{ss}),\\
\hat{H}_e &= -\frac{1}{2M}\sum_{i=1}^{N_e}\Delta_i + \sum_{i\neq j}^{N_e}\xi_0^{ee}u\left(\frac{|q_i-q_j|}{\lambda_{ee}}\right),\\
\hat{H}_{es} &= \sum_{i=1}^{N_e}\sum_{j=1}^{N_s}\xi_0^{es}u\left(\frac{|q_i-Q_j|}{\lambda_{es}}\right),\\
\hat{H}_{ss} &= \frac{1}{2M}\frac{m_e}{m_s}\sum_{j=1}^{N_s}\Delta_j + \sum_{i\neq j}^{N_s}\xi_0^{ss}u\left(\frac{|Q_i-Q_j|}{\lambda_{ss}}\right).
\end{aligned} \tag{21}$$

In the problem at hand we choose $m_e/m_s \sim 1/2000 \ll 1$, therefore, on the time scale t' the scatterers are practically fixed. $\hat{H}_{ss}$ is the Hamiltonian of the scatterers, and $\xi_0^{ee} = V_0^{ee}t'/\hbar$, $\xi_0^{es} = V_0^{es}t'/\hbar$ and $\xi_0^{ss} = V_0^{ss}t'/\hbar$ are the constants of the binary interaction between electrons (e-e) $u\,(|q_i-q_j|/\lambda_{ee})$, electrons and scatterers (e-s) $u\,(|q_i-Q_j|/\lambda_{es})$ and between scatterers (s-s) $u\,(|Q_i-Q_j|/\lambda_{ss})$, respectively. q_i represent the positions of the electrons ($i = 1,\ldots,N_e$), and Q_j those of the scatterers ($j = 1,\ldots,N_s$).

The (e-e), (e-s) and (s-s) interactions are taken in the form of the Kelbg potential [36, 37], which is the exact quantum pair potential of an ensemble of weakly nonideal and weakly degenerate charged particles:

$$u(|x_{ab}|) = \frac{1}{x_{ab}} \left[1 - e^{-x_{ab}^2} + \sqrt{\pi} x_{ab} \left(1 - \mathrm{erf}(x_{ab})\right)\right] \tag{22}$$

where $x_{ab} = |\mathbf{r}_{ab}|/\lambda_{ab}$, with λ being the thermal wave length given by $\lambda_{ab}^2 = \frac{\hbar^2\beta}{2\mu_{ab}}$, μ_{ab} the reduced mass $\mu_{ab}^{-1} = m_a^{-1} + m_b^{-1}$, $V_0^{ab} = \frac{e_a e_b}{\lambda_{ab}}$ and e_a, e_b being the respective charges. The $\mathrm{erf}(x)$ stands for the error function. Note that the Kelbg potential is finite at zero distances and coincides with the Coulomb potential at distances larger than λ_{ab}. This potential has recently been successfully applied to the computation of thermodynamic [25, 26, 27] and dynamic properties [38] of dense quantum plasmas by means of path integral Monte Carlo and classical molecular dynamics methods, respectively. It is, therefore, expected to provide an accurate description of the full Coulomb interaction between all particles within the quantum dynamics approach of the present paper.

Due to the large difference in the masses of electrons and heavy scatterers we can use two simplifications. The first one consists in the antisymmetrization of the density matrix only for electron spins and space coordinates. The second one, as we mentioned above, is the use of the adiabatic approximation for the dynamical evolution, where the positions of the heavy scatterers in each initial configuration were fixed during the electron-dynamics time given by the scale t'. The dynamic evolution has been realized according to relations (5), (6). Let us stress, that the Kelbg potential appearing in the canonical density operator used for ensemble averaging in (10) has to be taken at the inverse temperature $\epsilon \equiv \beta/2n$ while the simulation of the dynamic evolution, according to Eqs. (5,6) involves the Kelbg potential at the temperature $1/\beta$.

To simplify the computations we included in (12) only the dominant contribution to the sum over the total electron spin s corresponding to $s = N/2$ electrons having spin up and down, respectively. The contribution of the other terms decreases rapidly with particle number and vanishes in the thermodynamic limit. To further speed up the convergence of the numerical calculations we bounded the integration over the variables $q_M, q_1', q_M', \tilde{q}_1$ responsible for oscillations of the function φ in (11) and checked the insensibility of the obtained results to these operations.

IV. NUMERICAL RESULTS

We now apply the numerical approach explained above to the problem of an interacting ensemble of electrons and disordered scatterers in one dimension. In all calculations and figures times, frequencies and distances are measured in atomic units. The average distance between electrons, $R_s = 1/n_e a_0$, was taken to be $12.0; 2.6; 0.55$, the densities of electrons and heavy scatterers are equal. The results obtained were practically insensitive to the variation of the whole number of the particles in Monte Carlo cell from 30 up to 50 and also of the number of high temperature density matrices (determined by the number of factors n) in (10), ranging from 10 to 20. Estimates of the average statistical error gave the value of the order 5-7 percent. We studied two different temperatures: $k_B T/|V_0^{es}| = 0.45$ and 0.28, corresponding to $\lambda_{ee}/a_0 \sim 2.2$ and $\lambda_{ee}/a_0 \sim 3.5$, respectively. The strengths of the three interactions in the system are fixed arbitrarily at the ratio $V_0^{ee} : V_0^{es} : V_0^{ss} \sim 0.7 : 1 : 32$.

According to the Kubo formula [16] our calculations include two different stages: (i) the generation of the initial conditions (configuration of scatterers and electrons) in the canonical ensemble with probability proportional to the quantum density matrix and (ii) the generation of the dynamic trajectories on time scales t' in phase space starting from these initial configurations.

The results presented below are related to three different situations. The first two situations refer to the generation of initial configurations used for ensemble averaging, where the (e-e) interaction is fully included (called "interacting ensemble"), while the electron dynamics was simulated in case I. *with* (e-e) interaction ("interacting dynamics") and, in case II., *without* (e-e) interactions ("noninteracting dynamics"). For reference a third situation, III., was studied where the (e-e) interaction is neglected completely, i.e. both, in the initial ensembles ("noninteracting ensemble") and in the dynamical evolution, see also Fig. 1 for illustration. As we mentioned before to avoid the influence of (e-s) bound state effects we have considered only a system of negatively charged heavy scatterers here. The influence of (e-s) attraction on localization will be studied in a further publication.

A. Temporal quantum momentum-momentum correlation functions

First we discuss the influence of (e-e) interactions on the temporal quantum momentum-momentum correlation function. Fig. 2 shows momentum-momentum correlation functions corresponding to the situations I. and II. introduced above, i.e. to interacting ensembles with interacting (curves 1) and noninteracting (curves 2) dynamics,

respectively. Fig. 2 allows us to compare the obtained functions for two temperatures and densities varying over one order of magnitude.

The traces clearly show coherent oscillations, which are a manifestation of localization tendencies even at finite temperature. Note that at higher temperatures (right-hand panel) these oscillations are less pronounced compared to lower temperatures (left-hand panel). The damping times of these coherent oscillations are clearly different for the noninteracting and interacting dynamics. We observe that the electron-electron interaction leads to a strong reduction (curve 1) of this damping time as compared to (e-e) noninteracting electrons (curve 2). Furthermore, for the noninteracting dynamics the appearance of deep aperiodic modulations is seen. The dynamics of (e-e) noninteracting electrons leads to at least one large oscillation and several damped small ones, reflecting a strong spatial confinement of the electron system in this case. For interacting dynamics both, the first aperiodic modulation and the subsequent damped coherent oscillations are less pronounced.

The damping time for coherent oscillations increases with increasing density and decreasing temperature. The physical reason of this phenomenon is the tendency towards ordering of the scatterers, which is obvious from the corresponding pair distribution functions (g_{ss}) presented in Fig. 3, which develop periodic modulations for higher densities.

As an interesting side-result Fig. 4 presents the influence of the choice of initial conditions. In the left column we show the momentum-momentum correlation functions corresponding to situations II. and III., i.e. interacting (curves 1) and noninteracting (curves 2) ensembles and, in both cases, dynamics without electron-electron interaction. The analysis of the equilibrium configurations and pair distribution functions for the noninteracting ensemble (right column of Fig. 4) shows that the main contributions to the ensemble averaging result from absolutely different particle configurations if compared to the case of the interacting ensembles discussed above. The (e-e) noninteracting electrons are gathered mainly in the extended deepest potential well, while the heavy scatterers form a potential barrier confining the electrons. The typical initial configuration for equilibrium averaging, therefore, contains a so called 'electron bubble'. The (e-e) noninteracting electrons oscillate inside this 'bubble' with frequencies defined by the eigenvalues of the resulting potential energy profile of this well. On the other hand, for the typical configurations of interacting ensembles (cf. Fig. 3) the scatterers and electrons are both distributed more or less uniformly in space and the potential profile shows only spatial small-scale random inhomogeneities.

In the case of noninteracting ensembles we can see high frequency coherent oscillations with frequencies defined by the potential forming the 'bubble', while for interacting ensembles with their spatial small-scale potential profile only aperiodic oscillations (cf. Fig. 2, curves 2) are seen.

B. Fourier transform of the momentum–momentum time correlation functions

Figures 5 - 7 present the real and imaginary parts of the diagonal elements of the electrical conductivity tensor versus frequency, i.e. the real and imaginary parts of the Fourier transform of the temporal momentum–momentum correlation functions. The real part of the Fourier transform characterizes the Ohmic absorption of electromagnetic energy and has the physical meaning of electron conductivity, while the imaginary part presents $(\epsilon - 1)\omega$, where ϵ is the permittivity of the system.

Curves 1 and 2 of Fig. 5 show an opposite behavior for vanishing frequency. Most remarkably, the low-frequency conductivity related to the interacting dynamics (curve 1) is positive, while that for the noninteracting dynamics (curve 2) has a maximum at some finite frequency related to the coherent oscillations in the time domain. For lower frequency it changes sign. However, the real part of the conductivity has to be nonzero. The negative contributions are due to weakly damped very slow oscillations with time scales exceeding the scale t' considered for the calculation of the dynamics for the noninteracting dynamics (see the temporal momentum-momentum correlation functions, Fig. 2). To overcome this deficiency of our model one has to increase the time t' and/or to take into account the slow motion of the heavy particles, which will destroy the coherent oscillation of the light electrons trapped by the heavy particles and thus suppress these negative values. In fact, we found that calculations performed for longer and longer times lead to decreasing negative contributions for low frequencies.

Nevertheless, let us stress that the results obtained (Figs. 2 and 5) allow us to conclude that the behavior of the conductivity in the vicinity of zero frequency resembles the characteristic features of Anderson localization (i.e. a vanishing zero-frequency conductivity and enhanced oscillations related to the maximum in the real part at finite frequency) for noninteracting dynamics of electrons. The (e-e) interaction, on the other hand, leads to a strong increase of the conductivity at low frequencies and less pronounced oscillations.

Let us note that the high frequency tails of the real and imaginary parts of the Fourier transforms presented in Figs. 5 and 6 coincide with each other, as the main contribution is due to the fast trajectories with high virtual energy. This means, the (e-e) interaction does not influence the behavior of the high frequency tails. Furthermore, we have checked that the high- frequency tails of the real and imaginary parts of the Fourier transform can be described by

the Drude-asymptotics for free electrons. This reflects the fact that also the (e-s) interaction (its coupling constant being comparable to that of the (e-e) interaction) does not effect the behavior of the high-energy trajectories.

The Fourier transform of the correlation functions for noninteracting dynamics and both interacting and noninteracting ensembles are presented in Fig. 7 (cf. also Fig. 4). The most remarkable feature of these figures is the splitting of the peak related to the coherent electron oscillations for the noninteracting ensembles. The positions of the inserted triangles show the energy difference between subsequent eigenenergy levels calculated for an averaged bubble. The comparison of the peak and the triangle positions confirms the fact that [16] the Fourier transform of the momentum-momentum correlation function contains a sum of products of delta-functions and momentum matrix elements related to transitions between these energy levels. The imaginary part of the Fourier transform presented in the right column of Fig. 7 reflects that these characteristic features are related to the resonance oscillations in the 'bubble' mentioned above.

Figure 5 shows that for noninteracting dynamics, at low temperatures and moderate densities, e.g. $R_s = 2.6$ (cf. Figs. b), a well-resolved absorption peak appears which is related to the electron energy level separation. Note that this peak is present even in the case of interacting ensembles. However, there, the height of this peak is considerably smaller than in the case of noninteracting ensembles (Fig. 7).

C. Position dispersion

Finally, we discuss the position dispersion of electrons for interacting and noninteracting ensembles and noninteracting dynamics, cf. Fig. 8. Electron localization in the bubble results in a very slow growth (curve 2) of the position dispersion in comparison with the case of the small-scale potential profile (curve 1) of the initial configurations, as seen in Fig. 8. The square root of the position dispersion at times of the order of unity yields the typical size of the bubble. However, for larger times, $t > 80$, curve 2 shows a behavior, which is typical for particle diffusion. This characteristic change in behavior is due to the tail of the electron energy distribution function and is related to the fact that we are dealing with non-selfaveraging quantities. For the high-frequency tails of the Fourier transforms the virtual energy of the trajectories may be large. These exponentially rare fast trajectories can give an exponentially large contribution to the position dispersion, as the difference in positions of fast trajectories may be exponentially large at sufficiently large time. A similar problem connected with exponentially large contributions of exponentially rare events arises in the consideration of classical wave propagation in random media. There, it is well known [39] that in one-dimensional systems the dispersion of wave intensities is not self-averaging, as exponentially rare configurations of scatterers can give rise to exponentially large contributions of intensity at large distances from the wave source.

V. CONCLUSION

The Quantum-Dynamics-Monte-Carlo approach applied to a one-dimensional system of interacting electrons in an array of fixed random scatterers at finite temperature gives strong evidence for an enhancement of the quantum mobility of electrons due to their mutual long-range many-particle interaction and thus substantiates previous expectations drawn from schematic models.

As in our approach the temperature is taken to be nonzero, Anderson localization is not expected to show up in the results for noninteracting electrons in a strict sense. On the other hand, for the considered temperatures (comparable to or less than the coupling constant of the electron-scatterer potential) localization tendencies are clearly observable in this case. They manifest themselves both, in the low-frequency behavior of the momentum-momentum correlation function related to the conductivity of the electron system, and in coherent oscillations. For nonzero electron-electron interaction these localization tendencies are relaxed and the frequency- dependent correlation function has a form not unlike a Drude behavior. The high-frequency tails resemble a Drude-behavior of free electrons in all cases.

For initial conditions describing a noninteracting ensemble, the scattering centers form electron-bubbles which accomodate the [(e-e) noninteracting] electrons in their eigenstates and lead to well-defined coherent oscillations. In contrast, for configurations describing interacting ensembles, the scatterers and electrons are both distributed more or less uniformly in space and the potential profile shows only spatial small-scale random inhomogeneities. Then the dynamics of interacting electrons in this spatial small-scale random potential profile shows only fast damped oscillations with much smaller damping time if compared to noninteracting dynamics and results in an increased low-frequency conductivity.

The present work shows that it is possible to treat a system of many quantum particles interacting with each other via the long-range Coulomb potential in a numerically rigorous scheme. Here we have considered the heavy particles to be essentially immobile species. On the other hand, if their mass is being reduced they will take part

in the dynamics, and we then have a system resembling a plasma of, e.g., electrons and holes. Such calculations are presently under way and will be published shortly.

VI. ACKNOWLEDGMENTS

The authors thank B.L. Altshuler for stimulating discussions and valuable notes and the NIC Jülich for computer time. V. Filinov acknowledges the hospitality of the Graduate College "Optoelectronics of Mesoscopic Semiconductors" and the Department of Physics of the Philipps-Universität Marburg. This work is partly supported by the Max-Planck Research Prize of the Humboldt and Max-Planck Societies, by the Deutsche Forschungsgemeinschaft (DFG) through the Quantenkohärenz Schwerpunkt, and by the Leibniz Prize. I.V. acknowledges financial support from the Hungarian Research Fund (OTKA) under T029813, T032116 and T034832.

[1] E. Abrahams, P.W. Anderson, D.C. Licciardello, and T.V. Ramakrishnan, Phys. Rev. Lett. **42**, 637 (1979).
[2] S.V. Kravchenko et al., Phys. Rev. Lett. **77**, 4938 (1996).
[3] S. Das Sarma, and E.H. Hwang, Phys. Rev. Lett. **83**, 164 (1999)
[4] L.P. Lévy, G. Dolan, J. Dunsmuir, and H. Bouchiat, Phys. Rev. Lett. **64**, 2074 (1990); V. Chandrasekhar, R.A. Webb, M.J. Brady, M.B. Ketchen, W.J. Gallagher, and A. Kleinsasser, Phys. Rev. Lett. **67**, 3578 (1991).
[5] A. Schmid, Phys. Rev. Lett. **60**, 80 (1991); F. von Oppen and E.K. Riedel, *ibid.* 84; B.L. Altshuler, Y. Gefen, and Y. Imry, *ibid.* 88.
[6] M. Pollak and M.L. Knotek, J. Non-Cryst. Solids **32**, 141 (1979).
[7] M. Pollak, Phil. Mag. **42**, 799 (1980).
[8] D.L. Shepelyansky, Phys. Rev. Lett. **73**, 2607 (1994).
[9] T. Vojta, F. Epperlein, and M. Schreiber, Phys. Rev. Lett. **81**, 4212 (1998).
[10] M. Schreiber, F. Epperlein, and T. Vojta, Physica A **266**, 443 (1999).
[11] F. Epperlein, S. Kilina, M. Schreiber, S. Uldanov, and T. Vojta, Physica B **296**, 52 (2001).
[12] H. Overhof and P. Thomas, "Electronic transport in Hydrogenated Amorphous Semiconductors", Springer Tracts in Modern Physics, Vol. **114**, (Springer, 1998).
[13] P.A. Lee, and T.V. Ramakrishnan, Rev. of Mod. Phys. **57**, 287 (1985).
[14] D. Belitz, and T.R. Kirkpatrik, Rev. of Mod. Phys. **64**, 261 (1994).
[15] A,V. Chaplik, Zh. Eksp. Teor. Fiz. **60**, 1845 (1971) [Sov.Phys.JETP **33**, 997,(1971)].
[16] D.N. Zubarev, *Nonequilibrium statistical thermodynamics*, Plenum Press, New York/London 1974.
[17] V. Tatarskii, Sov. Phys. Uspekhi **26**, 311 (1983).
[18] V.S. Filinov, J. Mol. Phys. **88**, 1517, 1529 (1996).
[19] V.S. Filinov, Yu. Lozovik, A. Filinov, E. Zakharov, and A. Oparin, Physica Scripta **58**, 297, 304 (1998).
[20] R.P. Feynman, and A.R. Hibbs, *Quantum mechanics and path integrals*, McGraw-Hill, New York, Moscow 1965.
[21] V.M. Zamalin, G.E. Norman, and V.S. Filinov, *The Monte Carlo Method in Statistical Thermodynamics*, Nauka, Moscow 1977 (in Russian).
[22] B.V. Zelener, G.E. Norman, and V.S. Filinov, *Perturbation theory and Pseudopotential in Statistical Thermodynamics*, Nauka, Moscow 1981 (in Russian).
[23] V.S. Filinov, High Temperature **13**, 1065 (1975) and **14**, 225 (1976)
[24] B.V. Zelener, G.E. Norman, V.S. Filinov, High Temperature **13**, 650, (1975)
[25] Details on our direct fermionic path integral Monte Carlo simulations are given in V.S. Filinov, M. Bonitz, W. Ebeling, and V.E. Fortov, Plasma Phys. Contr. Fusion **43**, 743 (2001).
[26] V.S. Filinov, M. Bonitz, and V.E. Fortov, JETP Letters, **72**, 245 (2000), [Pis'ma v ZhETF, **72**, 361 (2001)].
[27] V.S. Filinov, V.E. Fortov, M. Bonitz, and D. Kremp, Phys. Lett. A **274**, 228 (2000).
[28] V.S. Filinov, V.E. Fortov, M. Bonitz, and P.R. Levashov JETP Letters, **74**, 384 (2001) [Pis'ma v ZhETF, **74**, 422 (2001)].
[29] A. Filinov, M. Bonitz, and Yu. Lozovik, Phys. Rev. Lett. **86**, 3851 (2001).
[30] I.M. Sobol, R. Messer (Translator) *Monte Carlo Methods*, Univ. Chicago Publisher, Chicago 1975.
[31] G. Ciccotti, C. Pierleoni, F. Capuani, V. Filinov, Comp. Phys. Commun. **121-122** , 452-459 (1999).
[32] V. Filinov, Yu. Medvedev, V. Kamskyi, J. Mol. Phys. **85**, 717 (1995).
[33] Yu. Lozovik, and A. Filinov, Sov. Phys. JETP, **88**, 1026 (1999).
[34] *The Monte Carlo and Molecular Dynamics of Condensed Matter Systems*, edited by K. Binder and G. Ciccotti, SIF, Bologna, 1996.
[35] *Classical and Quantum Dynamics of Condensed Phase Simulation*, edited by B. J. Berne, G. Ciccotti, and D. F. Coker, World Scientific, Singapore, 1998.
[36] G. Kelbg, Ann. Physik, **12**, 219 (1963); **13**, 354; **14**, 394 (1964).
[37] W. Ebeling, H.J. Hoffmann, and G. Kelbg, Beitr. Plasmaphys. **7**, 233 (1967) and references therein.

[38] V. Golubnychiy, M. Bonitz, D. Kremp, and M. Schlanges, Phys. Rev. E **64**, 016409 (2001).
[39] S. Gredeskul, and V. Freilikher, Usp. Fiz. Nauk **160**, 239 (1990).

FIGURES

Fig.1 Illustration of the Quantum-Dynamics scheme for computation of the correlation function $C_{FA}(\tau)$. The quantum general dynamics scheme generates particle trajectories (long arrows) in phase space $p-q$ starting from an initial state at $t=0$. The two arrows indicate different ensembles used for averaging over the initial states which do (do not) include e-e interaction: interacting ensemble, (noninteracting ensemble). At randomly chosen times $t_1,\ldots,t_i,t_{i+1},\ldots,t_K$, a pair of dynamic trajectories (short arrows) is propagated in positive and negative time direction, e.g. from t_i to $t_i+\tau/2$ and $t_i-\tau/2$, respectively. $C_{FA}(\tau)$ is averaged over all K trajectories. Bold (dashed) arrows indicate (non-)interacting dynamics including (neglecting) e-e interaction.

Fig.2 Temporal momentum-momentum correlation for interacting ensembles for the case of interacting (1) and noninteracting (2) dynamics. Temperatures are $k_BT/|V_0^{es}|=0.28$ (left panel: a,b) and $k_BT/|V_0^{es}|=0.45$ (right panel: c,d).

Fig.3 e-e, e-s and s-s pair distribution functions for the interacting ensemble, for the same parameters as in Fig. 2.

Fig.4 Left Column: Temporal momentum-momentum correlation functions for the case of noninteracting dynamics and interacting (1) and noninteracting (2) ensembles. Temperature is $k_BT/|V_0^{es}|=0.45$. Right Column: Pair distribution functions for the noninteracting ensembles.

Fig.5 Real part of the Fourier transform of the temporal momentum-momentum correlation functions of Fig. 2

Fig.6 Imaginary part of the Fourier transform of the temporal momentum-momentum correlation functions of Fig. 2.

Fig.7 Real part (left column) and imaginary part (right column) of the Fourier transform of the temporal momentum-momentum correlation functions of Fig. 4. Triangles indicate the transition energies between the lowest energy eigenvalues for an anlytical model for the deepest scatterer potential which traps the electrons (vertical coordinates of the triangles are arbitrary).

Fig.8 Electron position dispersion for noninteracting dynamics and interacting (1) versus noninteracting (2) ensembles, cf. Fig. 4.

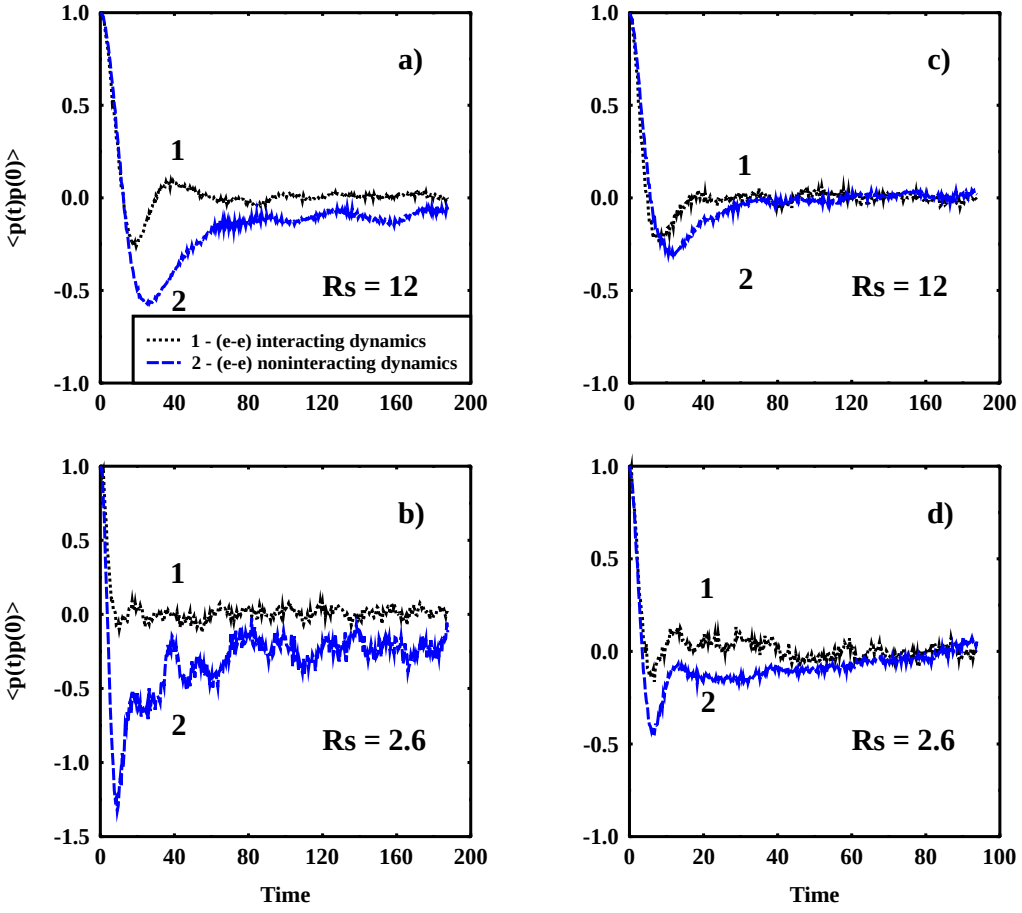
a)
b)
c)
d)
1
2
Rs = 12
Rs = 2.6
1 - (e-e) interacting dynamics
2 - (e-e) noninteracting dynamics
<p(t)p(0)>
Time

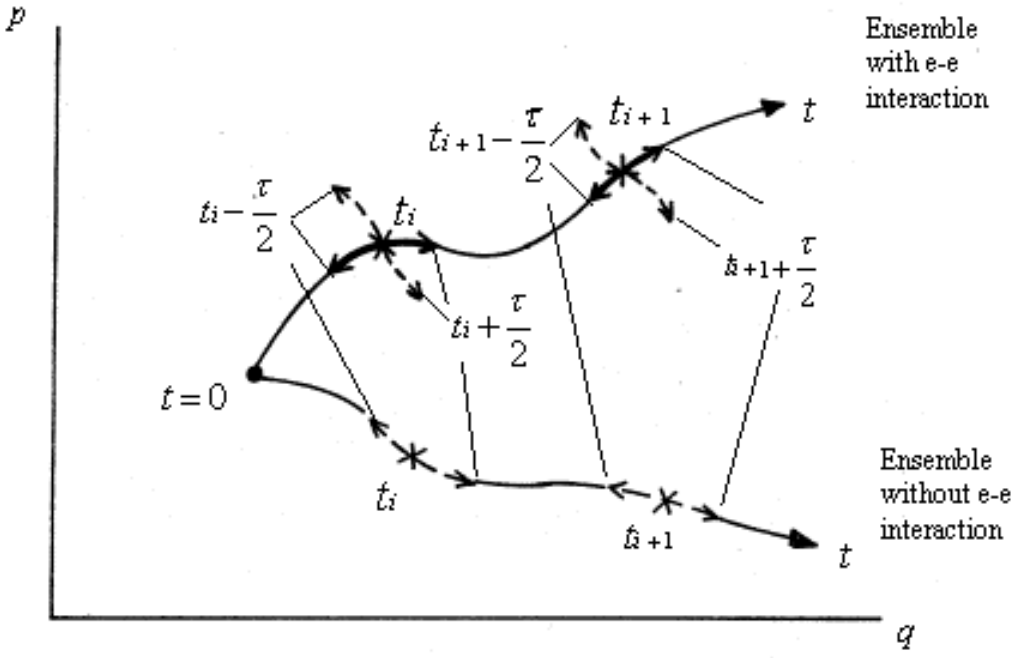
p
q
t
Ensemble with e-e interaction
Ensemble without e-e interaction
$t_i - \frac{\tau}{2}$
t_i
$t_i + \frac{\tau}{2}$
$t_{i+1} - \frac{\tau}{2}$
t_{i+1}
$t_{i+1} + \frac{\tau}{2}$
$t = 0$

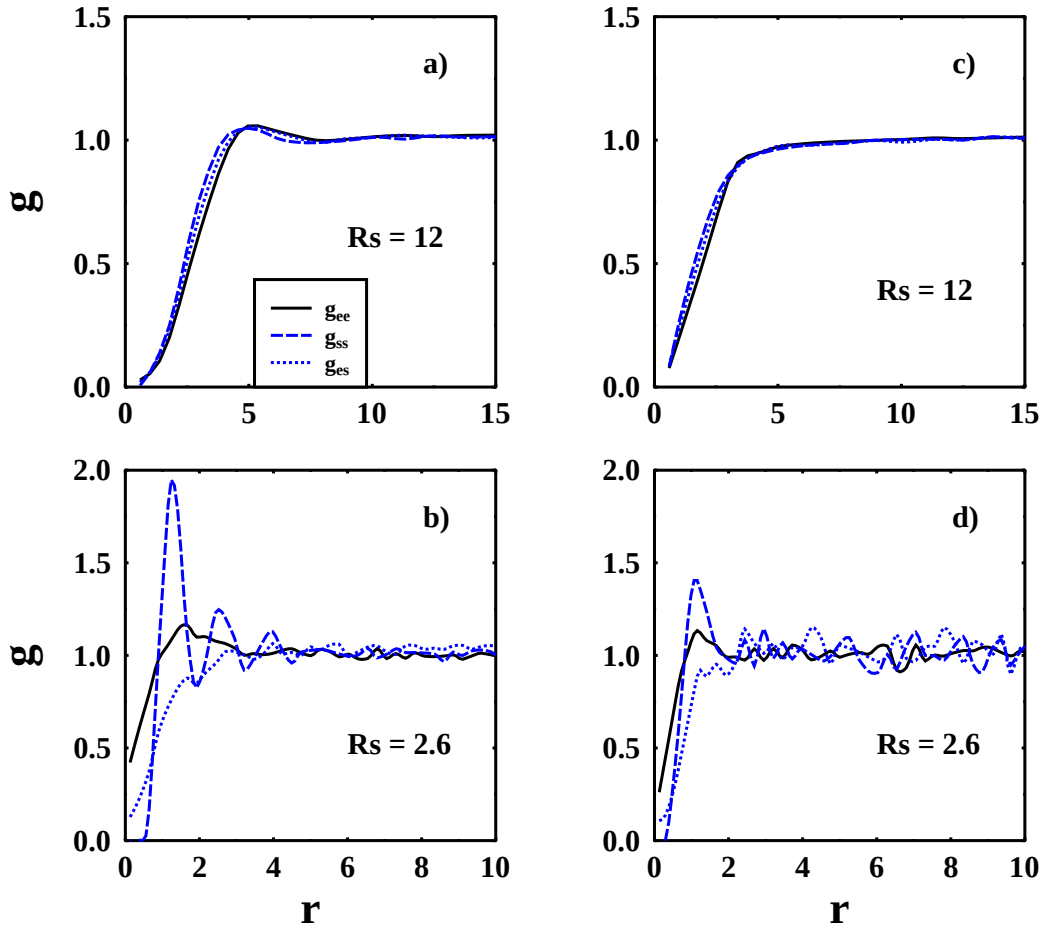
a)
Rs = 12
g_{ee}
g_{ss}
g_{es}
c)
Rs = 12
b)
Rs = 2.6
d)
Rs = 2.6
g
r
1.5
1.0
0.5
0.0
2.0
0
2
4
5
6
8
10
15

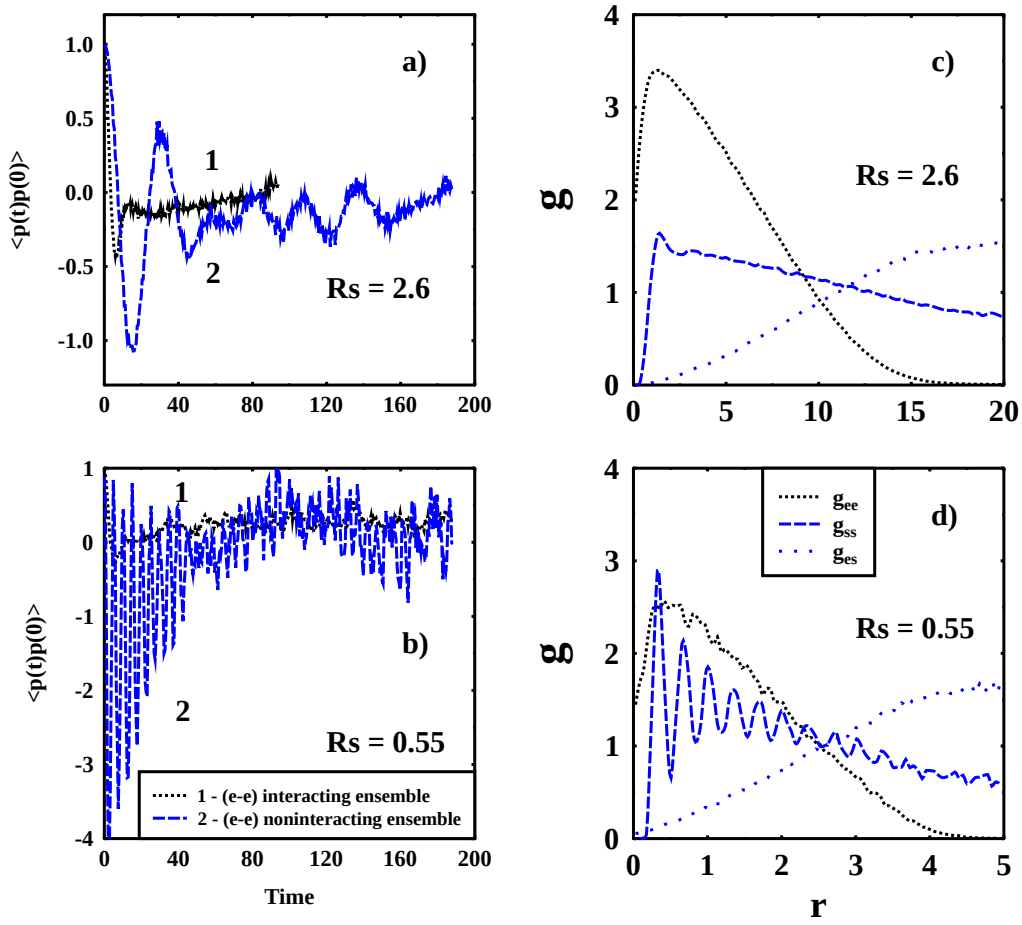
a)
1
2
Rs = 2.6
<p(t)p(0)>
b)
Rs = 0.55
1 - (e-e) interacting ensemble
2 - (e-e) noninteracting ensemble
Time
c)
Rs = 2.6
d)
Rs = 0.55
g
r

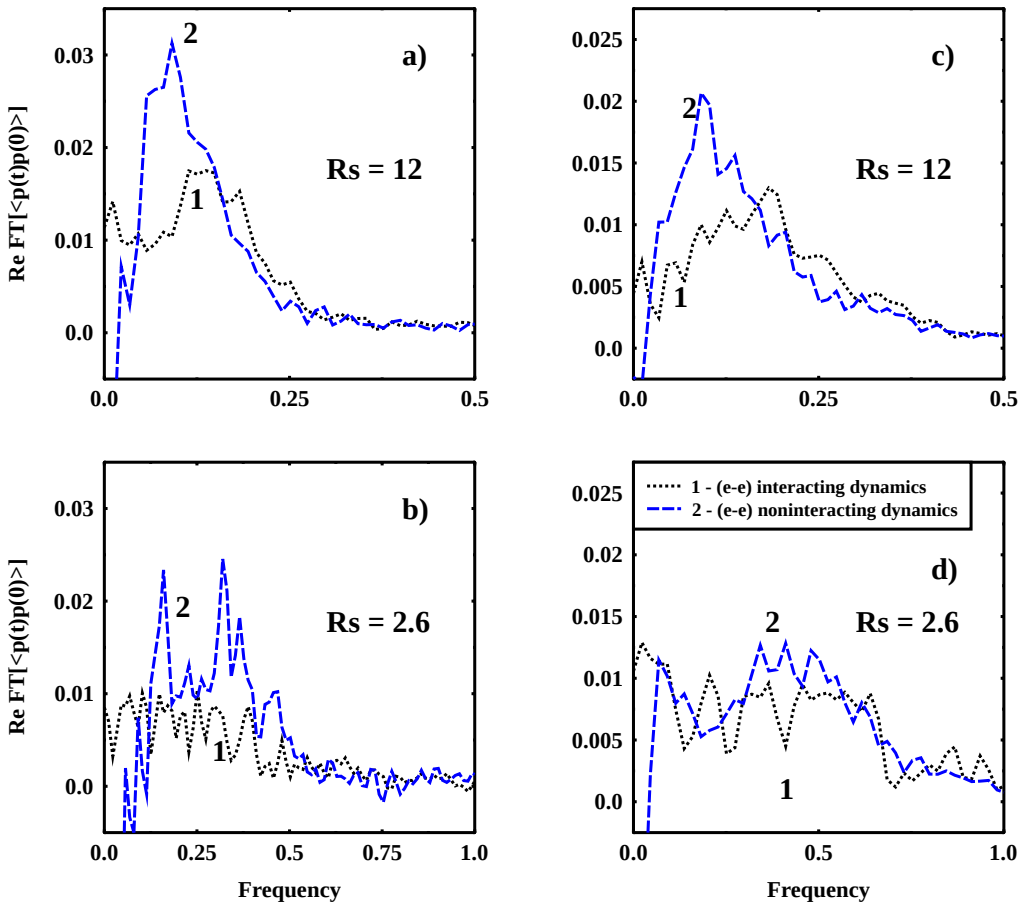
a)
Rs = 12
b)
Rs = 2.6
c)
Rs = 12
d)
Rs = 2.6
1 - (e-e) interacting dynamics
2 - (e-e) noninteracting dynamics
Re FT[<p(t)p(0)>]
Frequency

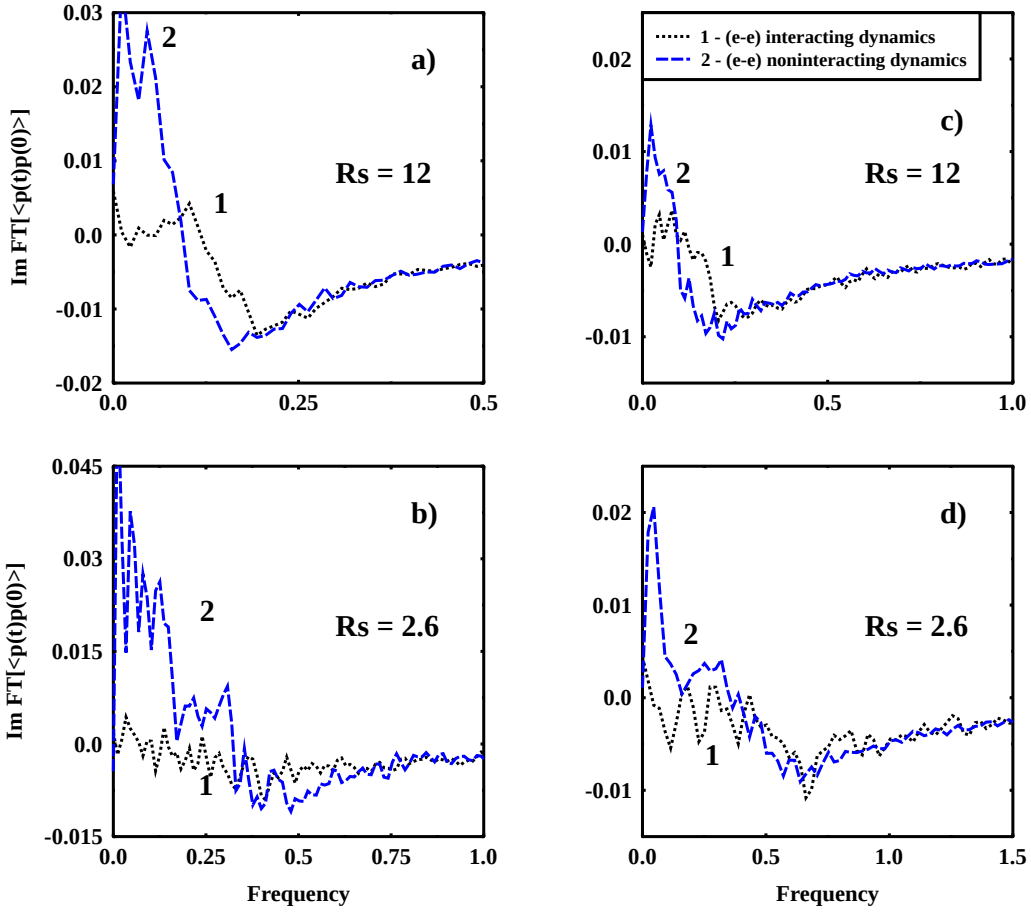
a)
Rs = 12
1
2
b)
Rs = 2.6
c)
Rs = 12
d)
Rs = 2.6
1 - (e-e) interacting dynamics
2 - (e-e) noninteracting dynamics
Im FT[<p(t)p(0)>]
Frequency

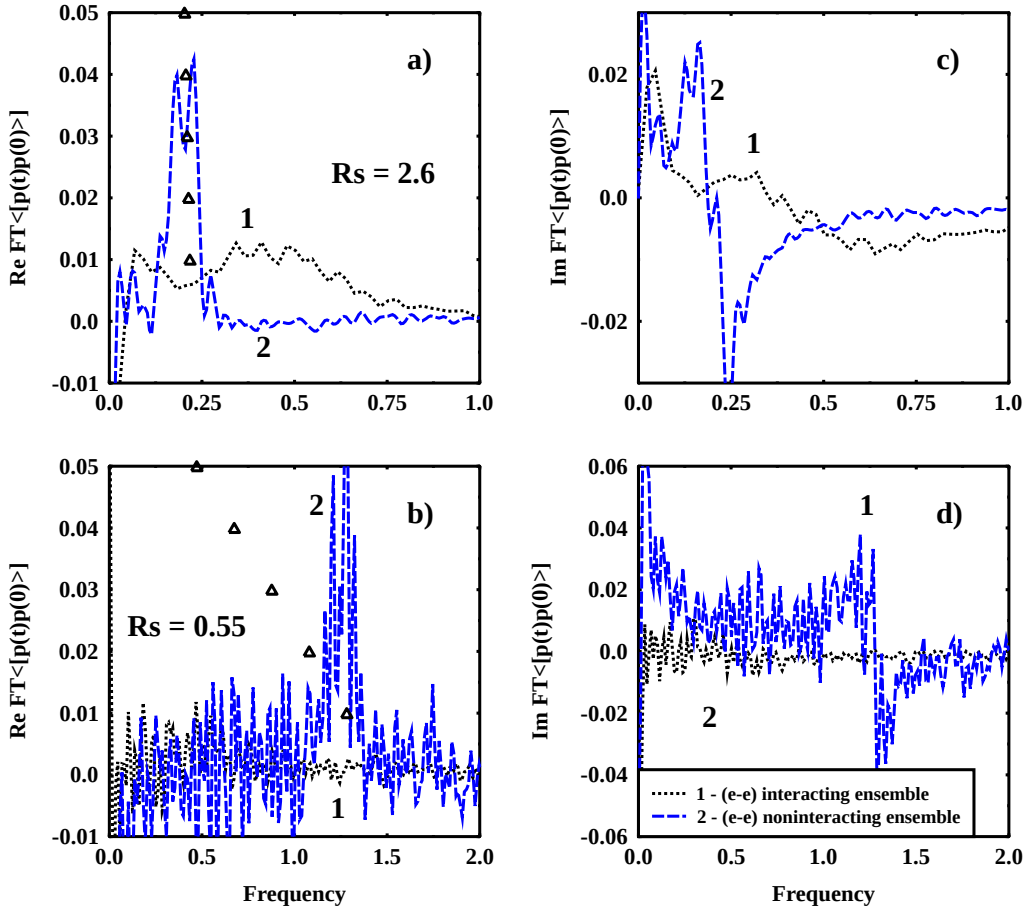
a)
Rs = 2.6
1
2
Re FT<[p(t)p(0)>]
c)
Im FT<[p(t)p(0)>]
b)
Rs = 0.55
Frequency
d)
1 - (e-e) interacting ensemble
2 - (e-e) noninteracting ensemble

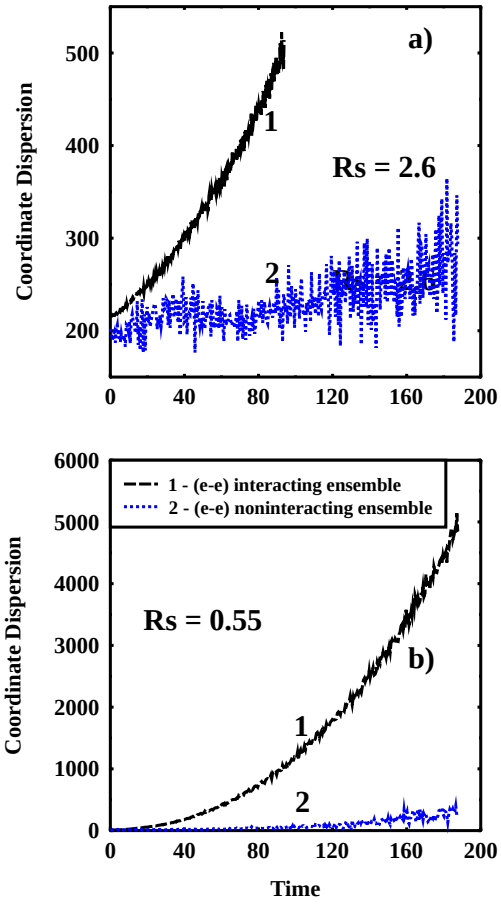
a)
1
2
Rs = 2.6
Coordinate Dispersion
500
400
300
200
0
40
80
120
160
200
1 - (e-e) interacting ensemble
2 - (e-e) noninteracting ensemble
Rs = 0.55
b)
1
2
Coordinate Dispersion
6000
5000
4000
3000
2000
1000
0
Time